Tutkimusraportti 63
Research Report 63

SIMULATION OF AMB SUPPORTED ROTOR DURING DROP ON RETAINER BEARINGS

Antti Y. J. Kärkkäinen
Jussi T. Sopanen
Aki M. Mikkola

ISBN 952-214-200-X (Paperback)
ISBN 952-214-201-8 (PDF)
ISSN 1459-2932

Lappeenranta University of Technology
Department of Mechanical Engineering
Institute of Mechatronics and Virtual Engineering
P.O.Box 20
FIN-53851 Lappeenranta
Finland

Lappeenranta, April 3, 2006

ABSTRACT

The active magnetic bearings present a new technology which has many advantages compared to traditional bearing designs. Active magnetic bearings, however, require retainer bearings order to prevent damages in the event of a component, power or a control loop failure. In the dropdown situation, when the rotor drops from the magnetic bearings to the retainer bearings, the design parameters of the retainer bearings have a significant influence on the behaviour of the rotor. In this study, the dynamics of an active magnetic bearings supported electric motor during rotor drop on retainer bearings is studied using a multibody simulation approach. Various design parameters of retainer bearings are studied using a simulation model while results are compared with those found in literature. The retainer bearings are modelled using a detailed ball bearing model, which accounts damping and stiffness properties, oil film and friction between races and rolling elements. The model of the ball bearings includes inertia description of rolling elements. The model of the magnetic bearing system contains unbalances of the rotor and stiffness and damping properties of support. In this study, a computationally efficient contact model between the rotor and the retainer bearings is proposed. In addition, this work introduces information for the design of physical prototype and its retainer bearings.

Keywords: Retainer bearing, Dropdown simulation, Ball bearing model, Contact model.

CONTENTS

1 INTRODUCTION

The area of Active Magnetic Bearings (AMBs) has recently been developed intensively because this non-contact support system has several advantages compared to conventional bearings. The most important advantages are almost non-existent friction and, because of that, little energy loss, no need for lubrication, quiet operation and adjustable stiffness and damping which makes accurate rotor positioning possible. In addition, AMBs offer almost unlimited control over the rotor that they support. Adjustable stiffness and damping become helpful especially from the mechanical point of view. Adjustable stiffness of the AMB makes it possible to decrease the natural frequencies of rotor's rigid body modes under the operation while, at the same time, the damping coefficient can be increased. As a consequence, the vibration at rigid body's natural frequency damps out, and the motor can be used at supercritical speeds. Furthermore, unbalance compensation during motor operation is possible due to active feedback control of AMB. In the unbalance compensation, the rotor does not rotate around its geometrical center but rotates around the centre of mass. It is obvious that this is not possible when using mechanical bearings. The most important mechanical parts in AMB are widely known. From outside to inside the main parts are the following; stator, electromagnets, and rotor laminations. Electromagnets, normally from 8 to 12 pieces in a stator, generate attraction which supports the rotor and, in principle, forces it to the center of the magnetic field. Function of the AMB's active part is easy to understand; a sensor measures location of the rotor in the air gap, and when the location deviates from the reference value, the controlling unit increases or decreases power of the AMB in order to achieve the reference value. In this way, the rotor levitates in the reference location. Unfortunately, this is only in theory, since gravity and unbalance forces make the design of control cumbersome leading to imperfect running of the rotor. Typically AMB application is expensive and unique due to high expense associated to development of control software. Compressors, generators, machine tools, and electric motors are the most general applications of AMB. Due to improved materials, strategies of controller, and electric components, the performance and reliability of AMB is enhancing. Despite of that, additional bearings, the so-called retainer bearings, have a vital role in the AMB applications. The most crucial moment when the retainer bearings are needed is when the rotor drops from AMBs to retainer bearings due to component or power failure [1, 2, 3]. Without any information and knowledge of retainer bearings, there is a great chance that AMB-rotor system will be suicidal on dropdown

situation. For this reason, the objective of this research is to shed light on the design of the retainer bearings.

Retainer bearings can be categorized into three types. Bushing type bearings are simple, and consequently, cheap and easy to repair if necessary. On the other hand, bushing type retainer bearings have some defects, which may restrict their use in some applications. Accordingly, the coefficient of friction can change during rotor's deceleration due to wearing of sleeve. Wearing typically increases the coefficient of friction and resulting to changes in the dynamic behavior of the rotor. For this reason, bushing type retainer bearings must be normally replaced for new ones after few number of high speed dropdowns. Secondly, based on low friction of coefficient, bushing type retainer bearings are unable to dissipate energy of the rotor without a whirling motion of the rotor. Retainer bearings of rolling element bearing type are more complicated and, therefore, they are also more sensitive for impacts. Rolling element bearing increases the power dissipation of the rotor during dropdown, because the inner race achieves rapidly the angular velocity of the rotor. This may prevent whirling motion of a rotor, as Fumagalli [4] noted. The last one type is a combination of those two mentioned above. This type of retainer bearing has some beneficial features as mentioned. However, this type suffers some drawbacks like a larger moment of inertia of rotating parts than rolling element bearing have.

The most examined characteristics of retainer bearings are the stiffness, damping and the friction coefficients between the rotor and bearing. Influences of those coefficients are widely known as pointed out by Ecker [5], Zeng [6], Ishii and Kirk [1]. Also force calculation and knowledge of the orbit of a rotor during contact are useful despite of the used bearing type, like Fumagalli [4] showed. Cole *et al.* [7] examined the dynamic behavior of rolling element bearing following rotor impact successfully. They pointed out that the inner race of the bearing should be allowed to accelerate as rapidly as possible in order to maximize the energy dissipation of the rotor. Raju *et al.* [8] did similar examination as Cole *et al.* [7] using solid brass backup bearings. Both of the results are useful, but only when designing similar retainer bearings as they examined. Dynamic behavior of bushing and rolling bearing type retainer bearings is different like Fumagalli's [4] and Swanson *et al.* [9] investigations proofed. This issue will be discussed later in this survey. In this topic, a number of inventive examinations have been done. For example, Wang and Noah [10] examined an accurate model of a sleeve auxiliary bearing during rotors dropdown. They concluded that the system should be designed

to avoid operation at the speed of the free-free eigenmodes of the rotor. This should be accounted in the dropdown situation, since it can lead to the chaotic behavior. That is why a non-linear dynamical analysis is critical for specific design of the rotor-retainer bearing system. Zeng [11] mentioned in his examination that the effect of decaying magnetic force of the failed AMB might be ignored in the simulations, because forces are not anymore significant. On the other hand, Orth *et al.* [3] compared the results of the Fumagalli's doctoral thesis with their own examinations and suggested that the reason for discrepancy was the collapsing magnetic field of the AMB's that was still producing decreasing magnetic force.

Common to all above mentioned examinations is that they are based on finite element model, rotor dynamic calculation or experimental studies. The objective of this work is to build a more accurate model of AMB system during the rotor dropdown using a multibody simulation approach. In addition, parameters of retainer bearings modified in order to find their contribution to the dynamic responses during the drop down. The retainer bearings are modelled by using a detailed ball bearing model, which includes damping and stiffness properties, oil film and friction between the races and rolling elements. The model also includes inertias of rotating parts. The inertias of the cage and the balls are combined. The model of the AMB system includes unbalances of the rotor and stiffness and damping properties of the support. Secondary objective of this work is to obtain of important information for the design the physical prototype and its retainer bearings.

2 DESIGN PARAMETERS OF BACKUP BEARING

Backup bearings' design parameters have significant effect on the dynamic behavior of the rotor during the dropdown. As a consequence, those effects must be known before the design of the backup bearings can be embarked. In this section, the most valid design parameters of backup bearings are studied with the help of literature. Design parameters will be studied also using numerical simulation later in this paper.

Stiffness of Bearing and Support

Wang and Noah [10] noted that the higher the bearing stiffness, the higher the full clearance backward whirling speed and the amplitude of whirling after dropdown of the rotor. They proposed that the bearing support stiffness can be selected at a value close to the stiffness of

the shaft in the auxiliary bearing design. Zeng [6] noted in his research that suitable soft support stiffness could reduce the nonlinear resonance and hence avoid whirling motion of the rotor. It is also good to remember that the vibration amplitude must be small enough to ensure that the rotor does not touch other parts of the assembly.

Damping of Bearing and Support

Ishii and Kirk [1] noted that in the cases of very low and high support damping, backward whirl occurs shortly after the rotor has dropped to the backup bearings. The backward whirl may lead to a large contact force. Therefore, the optimum support-damping ratio C_{bb}/C_{sh}, where C_{bb} is backup bearing damping and C_{sh} is unsupported shaft damping, is between 30 and 100. In this range, the backward whirl does not occur. Research made by Wang and Noah [10] showed also that an increase in the auxiliary bearing damping would help to reduce the whirling amplitude and eliminate the chaotic response.

Ishii and Kirk [1] noted that for small support damping ($C_{bb}/C_{sh} \leq 5$) the maximum rotor response and the maximum contact force are sensitive to the constraint in the rotational movement of bearing. These kind of constrains, like the nonlinearity of contact point, could exist for the AMB machinery, which operate for a long time without stops, because the backup bearings are inactive during the normal operation and, in some cases, highly preloaded.

Coefficient of Friction between Rotor and Retainer Bearing

Ecker [5] noticed that for large values of friction coefficients, the rotor starts backward whirling motion. This is important observation because often in magnetic bearing applications a contaminant free environment is required. This means that the auxiliary bearings are dry and thus without lubrication. Also Fumagalli and Schwitzer [12] noted that low coefficient of friction is a good feature for the retainer bearings. It is important to note that the coefficient of friction is not always constant. This is due to wear that can occur during the interaction between the rotor and retainer bearings and, thereby, increase the value of friction coefficient. A support with high stiffness will increase the friction coefficient rapidly and soon lead into full-clearance backward whirling motion of the rotor.

Sun [13] examined thermal growth of retainer bearing during the contact. He noted that rotor drop dynamics and thermal growth drastically change when the friction coefficient increases from 0.25 to 0.30. Because of larger friction force, orbit of a rotor extends after dropdown and

the first bounce direction becomes closer to the tangential direction of the contact point. Hence, it is important to find a threshold friction coefficient above of which rotor enters into high-speed backward whirl. Therefore, reducing the friction coefficient is so critical to the stability of the rotor drop dynamics. Fine surface finish and powder or solid lubricants can be utilized on the contact area, if it is acceptable in practice.

Thickness of Inner Race and Support Device's Mass

Cole *et al*. [7] used the finite element method to account flexibility of the inner race. They noticed that the peak loading of the rolling elements in a bearing can be reduced substantively by increasing the inner race thickness, thereby increasing the race stiffness. However, a thicker race will have a larger moment of inertia and, therefore, tends to accelerate more slowly. On the other hand, it would be preferable if the inner race accelerates as rapidly as possible in order to maximize the energy dissipation of the rotor, and to minimize the likelihood of friction induced rotor whirl.

Zeng [6] noticed in his research that suitable heavy backup device mass, i.e. mass of the retainer bearing assembly, could reduce the nonlinear resonances and hence avoid full clearance whirl motion of the AMB rotor that may lead to damage.

Balancing of Rotor

Kirk's [14] research concluded that a balanced rotor has a greater assurance that a drop will not initiate a violent whirl. He proved this analytically and experimentally. He also noted that the level of response tends to increase as the level of unbalance increases. For the hard-mount unlubricated solid bushing case, it was clear that violent backward whirling can occur for increased levels of unbalance.

Air Gap between Rotor and Retainer Bearing

Fumagalli [4] showed that the air gap between the rotor and retainer bearing should be large. He noted that, if the air gap is large enough, the rotor goes into pendulum like behavior rather than whirling motion. Normally, the clearance between the rotor and the retainer bearing is about half of the magnetic bearing's air gap. It is also important to note that the AMB's magnetic forces are inversely proportional to the square of the air gap. Thus, air gaps between the rotor and retainer bearing can not be chosen without restriction.

3 MODELS OF ROTOR AND BACKUP BEARING

Models of the rotor, bearings and contact are presented in this section. The model of the rotor is implemented in a commercial multibody software application [15] (MSC.ADAMS). The used model of the ball bearings is presented earlier by Sopanen and Mikkola [16, 17]. The bearing model is detailed, and because of that, useful for this application. Model of the contact, introduced in this study, can be used in mathematic programs as well as in multibody programs.

3.1 Model of the Rotor

In this paper, the rotor is modeled using a multibody simulation approach. In this approach, the motion of each body of the system is described using generalized coordinates. For body *i*, the vector of generalized coordinates, $\mathbf{q}_r^i$, can be written as [18]

$$\mathbf{q}_r^i = \begin{bmatrix} \mathbf{R}^{iT} & \boldsymbol{\theta}^{iT} \end{bmatrix}^T, \tag{1}$$

where $\mathbf{R}^i$ is the position vector of the origin of a local coordinate system of the body and $\boldsymbol{\theta}^i$ is the vector of generalized orientation coordinates. The orientation of the body can be described using, for example, Euler angles, Rodriguez parameters or Euler parameters. By using generalized coordinates, the global position of an arbitrary particle, *P*, on body *i* can be expressed in the following form:

$$\mathbf{r}^i = \mathbf{R}^i + \mathbf{A}^i \bar{\mathbf{u}}^i, \tag{2}$$

where $\mathbf{A}^i$ is a rotation matrix that describes the rotation of the local coordinate system with respect to the global coordinate system and $\bar{\mathbf{u}}^i$ is the position vector of a particle in the local coordinate system. The velocity of an arbitrary particle can be obtained by differentiating Equation (2) with respect to time as follows:

$$\dot{\mathbf{r}}^i = \dot{\mathbf{R}}^i + \dot{\mathbf{A}}^i \bar{\mathbf{u}}^i, \tag{3}$$

where $\dot{\mathbf{A}}^i \bar{\mathbf{u}}^i$ can be written as

$$\dot{\mathbf{A}}^i \bar{\mathbf{u}}^i = -\mathbf{A}^i \tilde{\bar{\mathbf{u}}}^i \bar{\mathbf{G}}^i \dot{\boldsymbol{\theta}}^i , \tag{4}$$

where $\tilde{\bar{\mathbf{u}}}^i$ is the skew symmetric matrix of vector $\bar{\mathbf{u}}^i$. Matrix $\bar{\mathbf{G}}^i$ defines the relationship between the angular velocities in the local body frame and the time derivatives of the orientation coordinates as follows:

$$\bar{\boldsymbol{\omega}}^i = \bar{\mathbf{G}}^i \dot{\boldsymbol{\theta}}^i . \tag{5}$$

It is important to point out that the expressions of the rotation matrix, $\mathbf{A}^i$, and matrix $\bar{\mathbf{G}}^i$ depend on the selected generalized orientation coordinates. By using Lagrange's equation and an augmented formulation for the kinematic constraints, the system equation of motion can be written as follows [19]

$$\mathbf{M}\ddot{\mathbf{q}} + \mathbf{C}_{\mathbf{q}}{}^T \boldsymbol{\lambda} = \mathbf{Q}_e + \mathbf{Q}_v , \tag{6}$$

where $\mathbf{M}$ is the mass matrix, $\mathbf{C}_{\mathbf{q}}$ the constraint Jacobian matrix, $\boldsymbol{\lambda}$ the vector of Lagrange multipliers, $\mathbf{Q}_e$ the vector of generalized forces and $\mathbf{Q}_v$ the vector of the quadratic velocity inertia forces. The mass matrix of body *i* can be obtained from the expression of the kinetic energy as follows:

$$T^i = \frac{1}{2}\int_{V^i} \rho^i \dot{\mathbf{r}}^{iT} \dot{\mathbf{r}}^i dV^i = \frac{1}{2} \dot{\mathbf{q}}_r^{iT} \mathbf{M}^i \dot{\mathbf{q}}_r^i , \tag{7}$$

where V^i is the volume of body *i*. The mass matrix, $\mathbf{M}^i$, can be written as follows:

$$\mathbf{M}^i = \begin{bmatrix} \mathbf{m}_{RR}^i & \mathbf{m}_{R\theta}^i \\ symm. & \mathbf{m}_{\theta\theta}^i \end{bmatrix}. \tag{8}$$

The submatrices can be written as follows

$$\mathbf{m}_{RR}^i = \int_{V^i} \rho^i \mathbf{I} dV^i = m^i \mathbf{I} \tag{9}$$

$$\mathbf{m}^i_{R\theta} = -\mathbf{A}^i \left[\int_{V^i} \rho^i \tilde{\bar{\mathbf{u}}}^i dV^i \right] \bar{\mathbf{G}}^i \tag{10}$$

$$\mathbf{m}^i_{\theta\theta} = \int_{V^i} \rho^i \bar{\mathbf{G}}^{iT} \tilde{\bar{\mathbf{u}}}^{iT} \tilde{\bar{\mathbf{u}}}^i \bar{\mathbf{G}}^i dV^i = \bar{\mathbf{G}}^{iT} \bar{\mathbf{I}}^i_{\theta\theta} \bar{\mathbf{G}}^i , \tag{11}$$

where $\mathbf{I}$ is a 3×3 identity matrix and $\bar{\mathbf{I}}^i_{\theta\theta}$ the inertia tensor of the body *i*.

The vector of quadratic velocity inertia forces, which contains the terms that are quadratic in the velocities, such as the gyroscopic and Coriolis terms, can be expressed as follows [18]:

$$\mathbf{Q}^i_v = \left[\left(\mathbf{Q}^i_v \right)_R \quad \left(\mathbf{Q}^i_v \right)_\theta \right]^T , \tag{12}$$

where vectors $\left(\mathbf{Q}^i_v \right)_R$ and $\left(\mathbf{Q}^i_v \right)_\theta$ can be written as

$$\left(\mathbf{Q}^i_v \right)_R = -\mathbf{A}^i (\tilde{\bar{\boldsymbol{\omega}}}^i)^2 \left[\int_{V^i} \rho^i \bar{\mathbf{u}}^i dV^i \right] + \mathbf{A}^i \left[\int_{V^i} \rho^i \tilde{\bar{\mathbf{u}}}^i dV^i \right] \dot{\bar{\mathbf{G}}}^i \dot{\boldsymbol{\theta}}^i \tag{13}$$

$$\left(\mathbf{Q}^i_v \right)_\theta = -\bar{\mathbf{G}}^{iT} \left[\tilde{\bar{\boldsymbol{\omega}}}^i \bar{\mathbf{I}}^i_{\theta\theta} \bar{\boldsymbol{\omega}}^i + \bar{\mathbf{I}}^i_{\theta\theta} \dot{\bar{\mathbf{G}}}^i \dot{\boldsymbol{\theta}}^i \right] . \tag{14}$$

The externally applied forces must be defined as generalized forces that affect the system's generalized coordinates. Using the principle of the virtual work, the generalized forces caused by globally applied forces, $\mathbf{F}^i$, and moments, $\mathbf{T}^i$, can be expressed as [18]

$$\left(\mathbf{Q}^i_e \right)_R = \mathbf{A}^i \mathbf{F}^i \tag{15}$$

$$\left(\mathbf{Q}^i_e \right)_\theta = \left(\mathbf{A}^i \bar{\mathbf{G}}^i \right)^T \left(\mathbf{A}^i \tilde{\bar{\mathbf{u}}}^i_P \mathbf{A}^i \mathbf{F}^i + \mathbf{A}^i \mathbf{T}^i \right) , \tag{16}$$

where $\left(\mathbf{Q}^i_e \right)_R$ and $\left(\mathbf{Q}^i_e \right)_\theta$ are the vectors of the generalized forces associated with the translational and rotational generalized coordinates of body *i*, respectively. Vector $\bar{\mathbf{u}}^i_P$ defines the working point of the force in the local coordinate system.

The kinematical constraint equations are functions of the system's generalized coordinates and can be expressed as follows:

$$\mathbf{C}(\mathbf{q}_r, t) = \mathbf{0}. \tag{17}$$

The constraint Jacobian matrix can be obtained by differentiating the constraint equations with respect to the generalized coordinates as follows:

$$\mathbf{C}_\mathbf{q} = \frac{\partial \mathbf{C}(\mathbf{q}_r, t)}{\partial \mathbf{q}_r}. \tag{18}$$

Equation (6) represents the dynamic equations of the constrained system. These differential algebraic equations (DAE) are nonlinear. Equation (6) is often solved through the use of the numerical integration approach of ordinary differential equations (ODE). To accomplish this, the constraint equations are differentiated twice with respect to time as follows [19]:

$$\mathbf{C}_\mathbf{q}\ddot{\mathbf{q}}_r = -\mathbf{C}_{tt} - (\mathbf{C}_\mathbf{q}\dot{\mathbf{q}}_r)_\mathbf{q}\dot{\mathbf{q}}_r - 2\mathbf{C}_{\mathbf{q}t}\dot{\mathbf{q}}_r. \tag{19}$$

By defining the vector $\mathbf{Q}_c$ as

$$\mathbf{Q}_c = -\mathbf{C}_{tt} - (\mathbf{C}_\mathbf{q}\dot{\mathbf{q}}_r)_\mathbf{q}\dot{\mathbf{q}}_r - 2\mathbf{C}_{\mathbf{q}t}\dot{\mathbf{q}}_r. \tag{20}$$

Equations (6) and (20) can be combined into one matrix equation as

$$\begin{bmatrix} \mathbf{M} & \mathbf{C}_\mathbf{q}^T \\ \mathbf{C}_\mathbf{q} & \mathbf{0} \end{bmatrix} \begin{bmatrix} \ddot{\mathbf{q}}_r \\ \boldsymbol{\lambda} \end{bmatrix} = \begin{bmatrix} \mathbf{Q}_e + \mathbf{Q}_v \\ \mathbf{Q}_c \end{bmatrix}. \tag{21}$$

The acceleration vector and the vector of Lagrange multipliers can then be solved from Equation (21).

3.2 Model of the Ball Bearing

Sopanen and Mikkola [16] presented a dynamic model of a deep-groove ball bearing using six degrees of freedom. The model of the bearing included descriptions of non-linear Hertzian contact deformation and elastohydrodynamic (EHD) fluid film thickness. The geometry, such as outer and inner diameter of bearing and clearances, and material properties are given as an

input to the model. The bearing force and torque components are calculated from the relative displacements and velocities between bearing rings. The torque around the rotation axis of the bearing is caused by friction and consists of three components; viscous friction torque, load-dependent friction torque and seal friction. In their study, the friction torque was found to play an insignificant role in terms of contact forces and responses. For the practical point of view this means that it is useful to select a sealed ball bearing as the retainer bearing. The sealed bearings are more protected for pollution than the normal ones and because of that potentially better for dropdown situation than normal bearings.

A single ball bearing consists of a number of moving parts and when describing responses of each part, the simulation model have a large number of degrees of freedom and for this reason it will be computationally expensive. Therefore, the model proposed by Sopanen and Mikkola is simplified as follows: Firstly, they did not notice the centrifugal forces of the balls. Furthermore, the cage of the bearing was assumed to be ideal. It means that the cage holds the balls in their predefined positions precisely. Thirdly, the bending deformation in the rings was assumed to be negligible. The last assumption was that no slipping or sliding occurs between the components of the bearing. This assumption may not be true all the time, especially in case of the retainer bearings, but it makes the determination of the bearing model significantly easier. However, despite of above-mentioned assumption, the force-deflection relationship was fairly complex.

3.3 Model of the Contact

Usually commercial multibody programs, such as MSC.ADAMS, includes built-in contact models [15]. That kind of contact is usually created to be generalized and multipurpose and therefore, calculation of contact may require significantly calculation capacity. Thus, it is important to create a contact model that works effectively and foreseeable every moment during the simulation. In addition, in this way it is possible to create friction model without insignificant parameters. For example, if slip velocity is always larger than the stiction transition velocity, it is not necessary to define the static friction coefficient.

Contact between the rotor and the bearing is modeled using a circle-in-circle contact which is presented in Figure 1. The radial contact F_r is a function of the contact penetration and the penetration velocity. The radial contact force, which affects on the rotor, can be written as follows

$$F_r = -1.0 \cdot \max \begin{cases} K(e_r - c_d)^e + f(e_r, c_d, 0, d, C) \cdot \dot{e}_r \\ 0.0 \end{cases}, \tag{22}$$

where K is stiffness of the contact and C is, respectively, damping of the contact. The exponent e is the force-deflection relationship. The X- and Y-components of the radial contact force F_r can be calculated using the geometry presented in Figure 1. Radial displacement, e_r, and velocity, $\dot{e}_r$, between the rotor and the sleeve can be obtained from the displacements along X and Y axes as follows

$$e_r = \sqrt{e_x^{\,2} + e_y^{\,2}} \tag{23}$$

$$\dot{e}_r = \frac{e_x \dot{e}_x + e_y \dot{e}_y}{\sqrt{e_x^{\,2} + e_y^{\,2}}}. \tag{24}$$

Clearance in the contact, c_d, is obtained from radiuses of the rotor r and the sleeve R as follows

$$c_d = R - r. \tag{25}$$

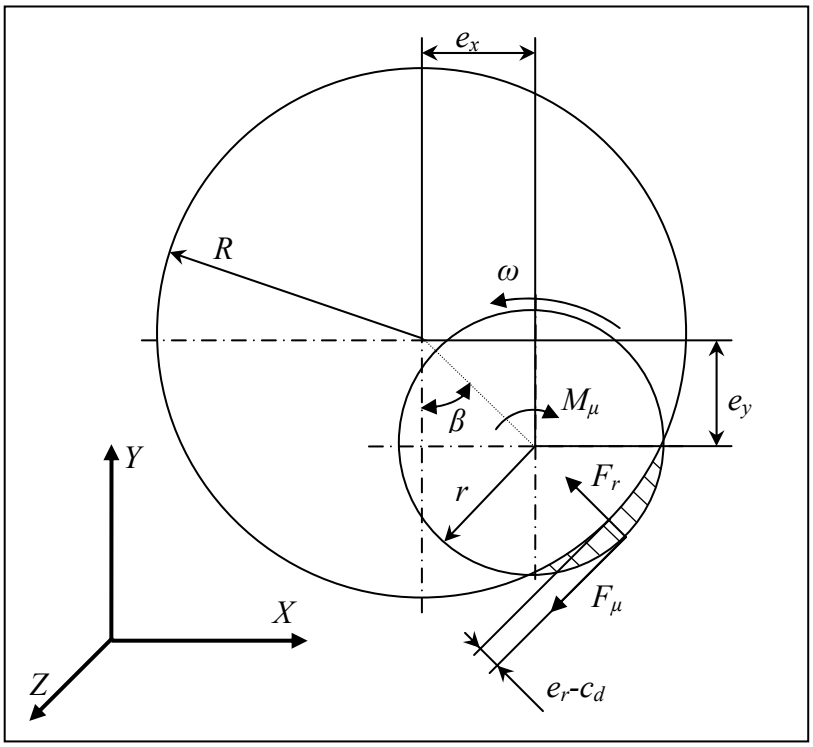

Fig. 1 Circle-in-circle contact.

To avoid discontinuities in the contact force, the velocity-dependent terms are smoothed using *step* function, which is defined by Equation (26). Thus, at zero penetration, the damping coefficient, C, is zero. The parameter d in Equation (22) is the radial displacement when a maximum damping coefficient is achieved. The step function employs cubic polynomials. The function is continuous for first derivatives and it is defined as

$$f(g, g_0, h_0, g_1, h_1) = \begin{cases} h_0 & ;\ g \le g_0 \\ h_0 + \Delta h \cdot \Delta g^2 (3 - 2\Delta g) & ;\ g_0 < g < g_1 \\ h_1 & ;\ g \ge g_1 \end{cases}, \tag{26}$$

where $\Delta h = h_1 - h_0$ and $\Delta g = \dfrac{g - g_0}{g_1 - g_0}$. Variable g is an independent variable, while g_0 and g_1 are the starting and ending values of the step. Correspondingly, h_0 and h_1 are the initial and final value of the function.

Magnitude of friction force, which acts to the center of the rotor and is perpendicular to the radial contact force, can be calculated as follows

$$F_\mu = \frac{\omega_{diff}}{|\omega_{diff}|} \cdot \mu \cdot F_r \cdot f(\omega_{diff}, 0, 0, \omega_l, 1), \tag{27}$$

where μ is the coefficient of friction between the rotor and bearings. Parameter ω_{diff} describes the difference of angular velocities between the rotor and the sleeves and can be written as $\omega_{diff} = |\omega_r - \omega_s|$, where ω_r and ω_s are the angular velocities of the rotor and the sleeves. The parameter ω_l describes the threshold angular speed above which the friction coefficient μ achieves the maximum value. Because the friction force is assumed to act into the center of the rotor, it causes a torque which direction is opposite to the direction of rotation and can be defined as

$$M_\mu = F_\mu \cdot r. \tag{28}$$

4 STUDIED STRUCTURE

Studied structure is an electrical motor, whose rotor is supported by two Active Magnetic Bearings (AMBs). The structure includes also retainer bearings (6016 type, deep-groove ball bearing), which have a vital role in the case of emergency dropdown. The test rotor can be seen in Figure 2. Both AMBs (AMB_1 and AMB_2 in Figure 2) generate independent support forces F_{AMB1} and F_{AMB2}. Both support forces will be closing down immediately when a fault situation occurs, which means that the collapsing magnetic field will not generate any forces at all. On the inner rings of retainer bearings (RB_1 and RB_2 in Figure 2) are sleeves that are rigidly connected to the inner rings of the bearings. The air gap between the sleeve and the rotor is half of the air gap of AMB. Width of the sleeves is same as the width of the bearings. The outer rings of the retainer bearings are rigidly mounted to the bearing housings. For reason of simplify, the bearing housings have only two degrees of freedom, namely translations in the global *X*- and *Y*-directions. The housings are connected to the ground with linear spring-dampers in *X*- and *Y*-directions. The stiffness coefficients are the same in both directions, as well as the damping coefficients. The dimensions of the motor are shown in Table 1 and properties of the used retainer bearings are shown in Table 2. The direction of gravity *g* is the negative *Y*-direction. Unbalance mass UB is located at the middle of the rotor at an angle of 90º from the positive *X*-axis and at distance of 97.5 mm from the rotation axis. The parameters of the contacts between the rotor and the sleeves are shown in Table 3.

The rotor has six degrees of freedom and it is made of steel which density ρ is 7801 kg/m^3. In the simulation the axial motion in the *Z*- direction is prevented by using a spring. The rotor's rotational velocity *n* is 10 000 rpm (166.67 Hz) around the *Z*-axis in counterclockwise direction. The translational displacements and forces are measured from the both retainer bearings. Simulation data is recorded at a frequency of 20 000 Hz. Numerical integrator used here is Gear Stiff with an error tolerance of $1.0 \cdot 10^{-3}$ and a maximum time step of $1.0 \cdot 10^{-4}$ s. The model of the electric motor has 27 degrees of freedom.

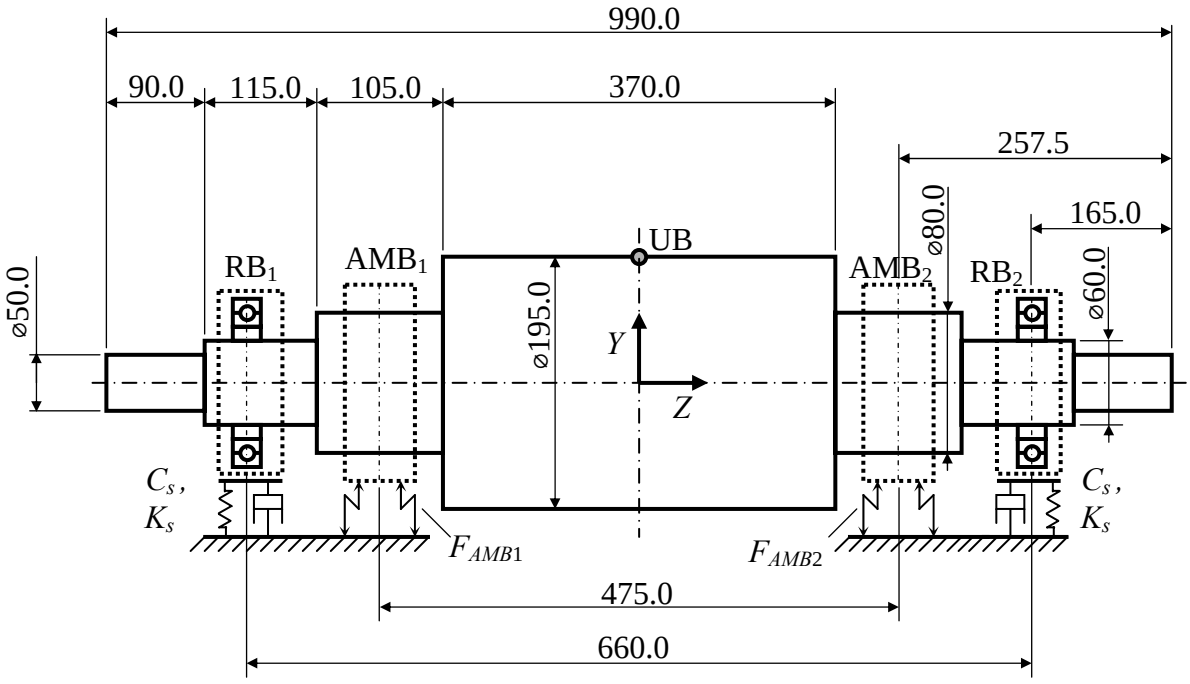

Fig. 2 Diagram of the electric motor under investigation. Dimensions are in millimeters.

Table 1 Parameters of the studied electric motor

Mass of the rotor, m	97.3 kg
Polar moment of inertia of the rotor, I_p	0.39 kgm^2
Diameter moments of inertia of the rotor, I_d	2.82 kgm^2
Air gap between rotor and sleeves	300 μm
Inner diameter of sleeve, d_{si}	60.6 mm
Outer diameter of sleeve, d_{so}	80.0 mm
Gravity constant, g	9.80665 m/s^2

Table 2 Parameters of the type 6016 retainer bearing

Bore diameter, d_B	80.0 mm
Outer diameter, D_O	125.0 mm
Bearing width, B	22.0 mm
Pitch diameter, d_m	110.0 mm
Ball diameter, d	19.05 mm
Number of balls, z	10
Diametral clearance, c_d	15 μm
Bearing damping coefficient, c_b	0.25 Ns/mm
Inner and outer race conformity, R_r	0.52
Static load rating, C_0	40 000 N
Modulus of elasticity, E	206 000 MPa
Poisson's ratio, v	0.3
Viscosity parameter, α	0.023 mm^2/N
Viscosity parameter, η_0	0.04·10^{-6} Ns/mm^2

Table 3 Parameters of the contact

Stiffness coefficient of the contact, K	$1 \cdot 10^8$ N/m
Damping coefficient of the contact, C	1000 Ns/m
The contact parameter, d	0.01 mm
Exponent of the force-deflection relationship, e	1.1
Threshold angular speed, ω_l	10 rpm

5 SIMULATION RESULTS

In this chapter, the effects of the friction coefficient and the mass of unbalance are studied. Effects of the stiffness and the damping coefficients of support to responses and contact forces are also examined. The total time of the simulation is 1 second and AMB's are turned off when the simulation is preceded 0.1 seconds. Initial angular velocity of the rotor is 10000 rpm.

5.1 Effect of Friction Coefficient

In this section the responses, the orbit of the rotor, the contact forces of the support, and the velocities of the sleeve are studied with different friction coefficients μ in these examples. The unbalance mass, m_{UB}, is 1 g, the stiffness of the support, K_s, is $5 \cdot 10^7$ N/m and the damping of the support, C_s, is 5000 Ns/m. Figure 3 shows the responses of the rotor at the retainer bearing 1. The rotor started to whirl when the friction coefficient between the rotor and the sleeves is 0.39. In Figure 4, the responses are presented in the case of friction coefficient of 0.40. The orbits of the rotor in various conditions are presented in Figures 5 and 6. Figures 5 and 6 show that the orbit of the rotor becomes larger as the friction coefficient increases. This can be seen even before the rotor starts to whirl. In the whirling motion, the orbit of the rotor increases significantly. The largest motion does not occur immediately after the dropdown, like in the cases of lower friction coefficients. The largest responses occur after 0.08 seconds of the dropdown. After this moment, the responses, i.e. the orbit of the rotor, are stabilizing. The orbit of the rotor does not stay inside of the static retainer bearing, the circle in Figures 5 and 6, after the dropdown. This is due to fact that the retainer bearings are assembled elastically to the ground and the bearing model describes compression of the bearing as well.

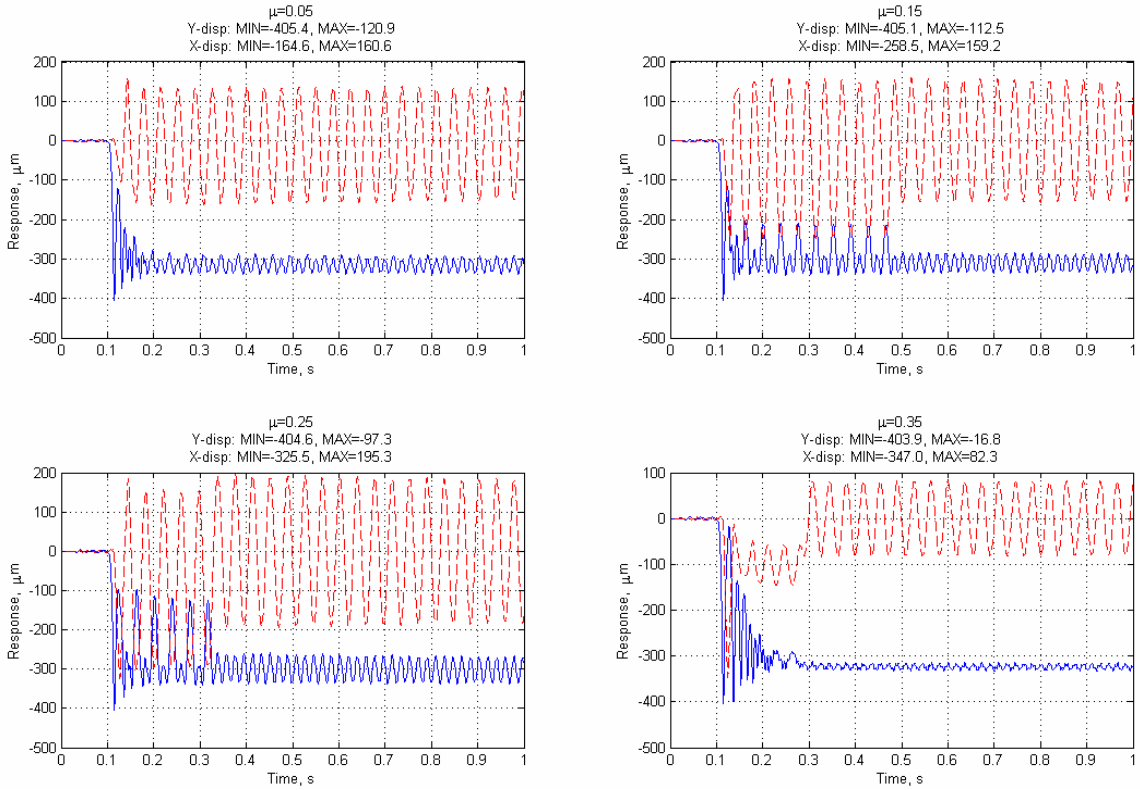

Fig. 3 Responses of the rotor. Solid line indicates *Y*-axis and dash line *X*-axis.

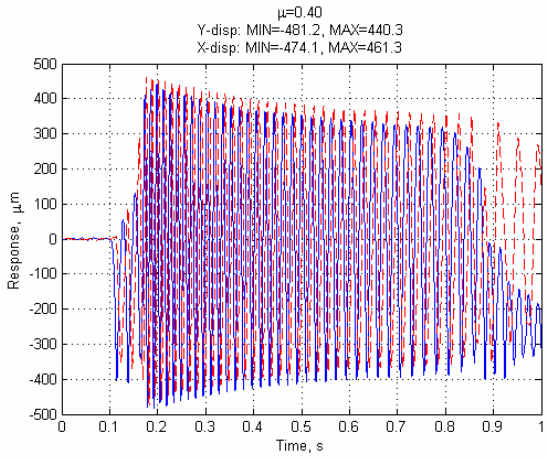

Fig. 4 Response of the rotor when the rotor goes into backward whirling motion. Solid line indicates *Y*-axis and dash line *X*-axis.

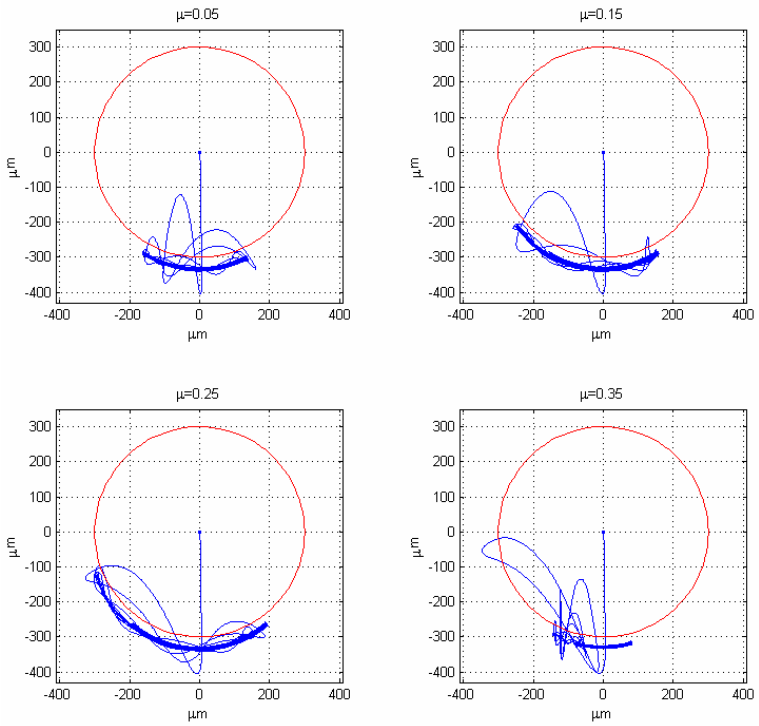

Fig. 5 Orbits of the rotor.

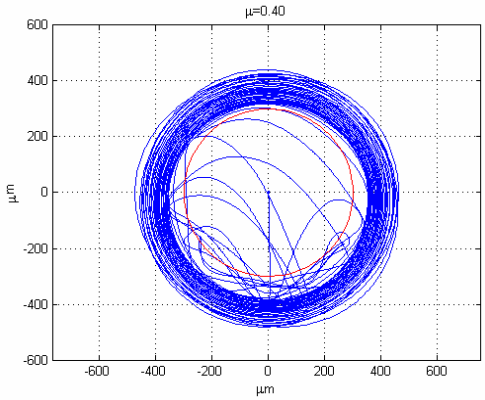

Fig. 6 Orbit of the rotor when the rotor goes into backward whirling motion.

The coefficient of friction has a vital role for contact forces if the rotor experiences a violent backward whirl, as can be seen in Figures 7 and 8. If the rotor stays at the bottom of the sleeves, the contact forces are approximately same during the deceleration in all cases. However, when the rotor started to whirl the contact forces increase significantly; the forces are two times larger than in the case where the rotor stays at the bottom of the sleeves. This should be accounted in mechanical design.

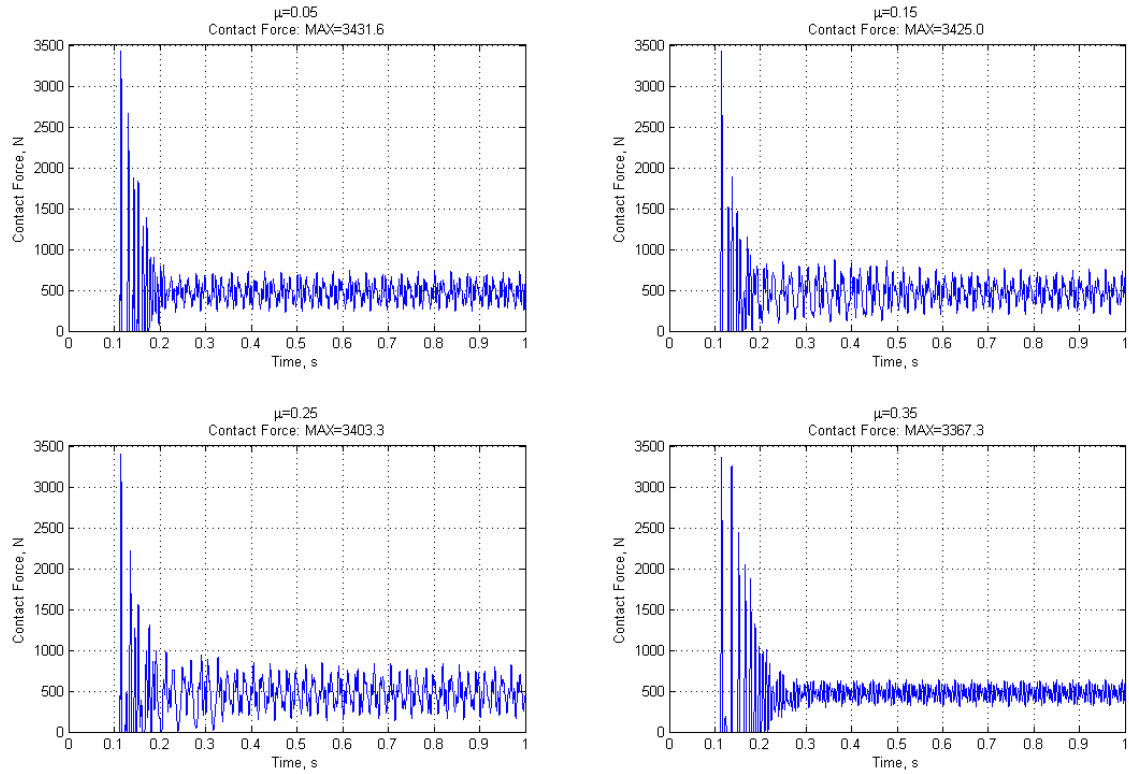

Fig. 7 Contact forces of the support.

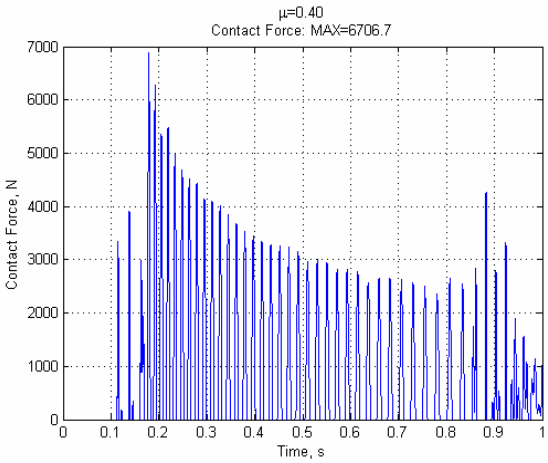

Fig. 8 Contact force of the support when the rotor goes into backward whirling motion.

Angular velocities of the sleeves are presented in Figures 9 and 10. Angular velocity depend on two parameters; the friction coefficient and the skid between the sleeves and the rotor. If the discrepancy between rotation velocities of the rotor and the sleeves is large, the sleeve accelerates more rapidly than if its rotation velocity is near to rotation velocity of the rotor. When the rotor starts to whirl, the sleeves accelerate much faster than in the case when the rotor stays bottom of the sleeves. The reason for this kind of behavior is the constant contact between rotor and sleeves. Immediately after the dropdown, the rotor bounces back and forth as can be noted in Figures 5 and 6. This behavior causes steps to the curve describing angular

velocities of sleeves. This can be seen especially in such situation where the rotor becomes to whirl (Figure 10). In the simulation, it is assumed that the friction coefficient between the rotor and the sleeves is the same all of the time during the simulation. This may be unreal, because friction coefficient changes depending of rotor's and sleeves' temperatures and wearing.

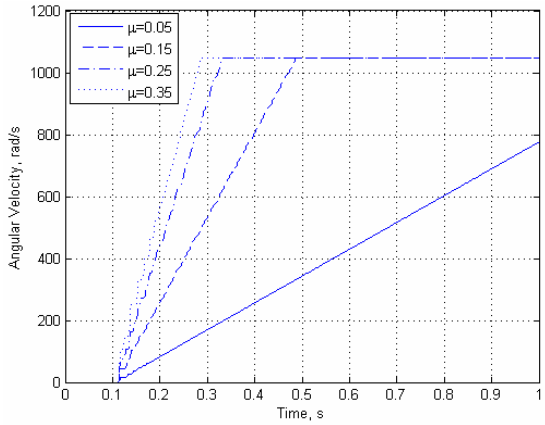

Fig. 9 Angular velocities of the sleeves.

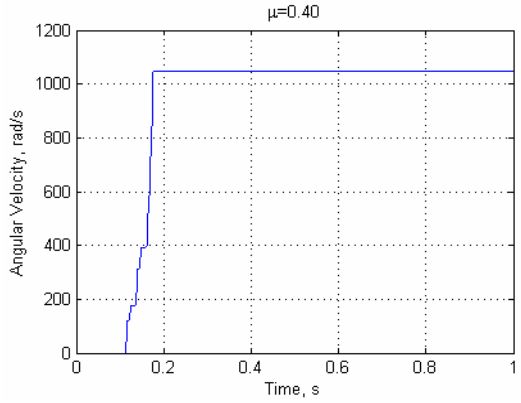

Fig. 10 Angular velocity of the sleeve when the rotor goes into backward whirling motion.

5.2 Effect of Mass of Unbalance

Figures 11, 12 and 13 show effects of the unbalance on responses, orbits, and contact forces. Variations of the unbalance are 5 and 10 grams. The value of the coefficient of friction is 0.25 all of the time when effects of unbalance are examined. The other parameters remain same. Figures 11 and 12 present that the mass of unbalance affects the behavior of the rotor, but do not change it significantly. It can be concluded from the results that larger mass of unbalance makes the orbit of the rotor more unexpected, chaotic, at this time. Also a vibration grows depending on mass of unbalance. This can be seen clearly in Figure 12 and 13. Figure 13 presenting the contact forces between rotor and sleeves shows that in the case of m_{UB}=5 g the contact forces are during the first drop larger than in the case of m_{UB}=10 g. The reason for this

kind of behavior is a phase angle of unbalance which affects the behavior of the rotor, like Swanson *et al.* noted in their examination [9]. After the drop down the contact forces are larger when m_{UB}=10 g which is expected.

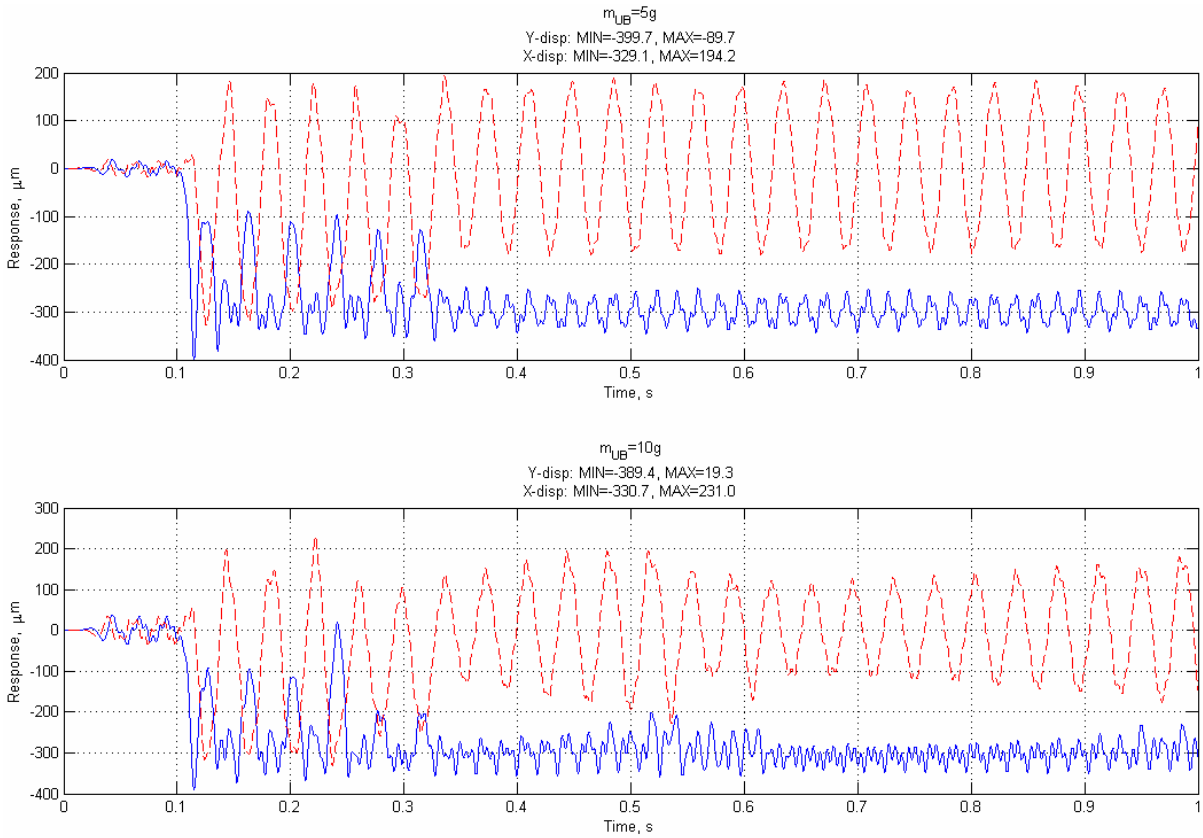

Fig. 11 Responses of the rotor with various mass of unbalance. Solid line indicates *Y*-axis and dash line *X*-axis.

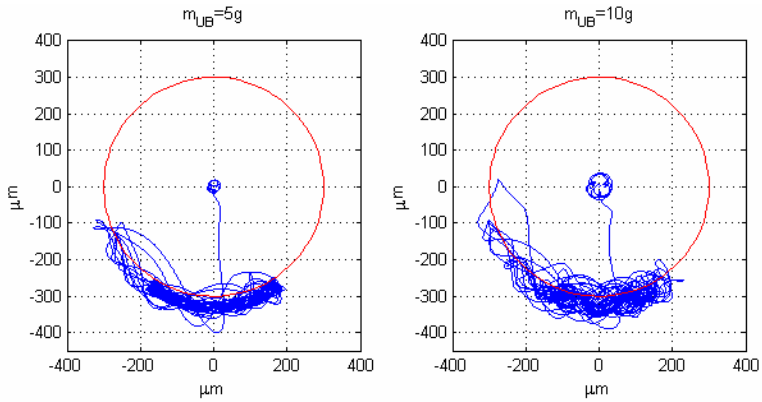

Fig. 12 Orbits of the rotor with various mass of unbalance.

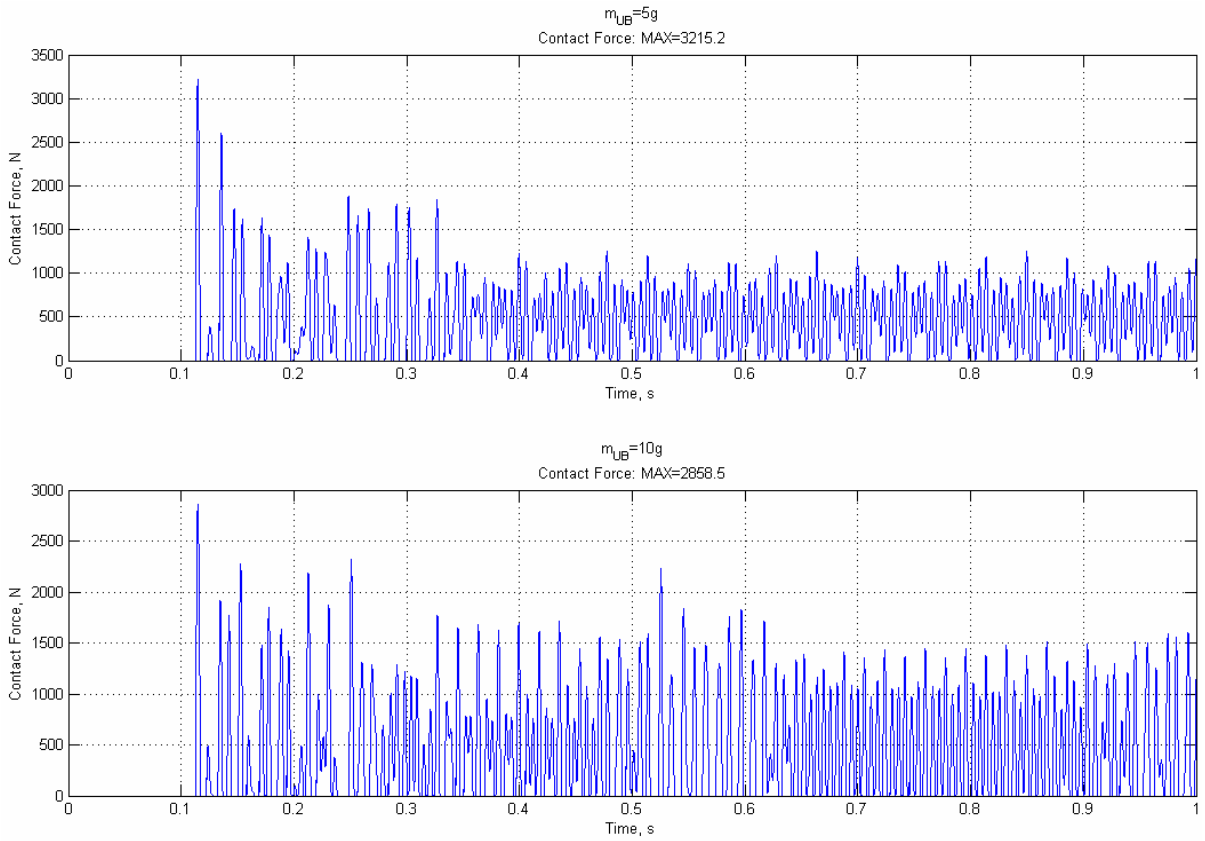

Fig. 13 Contact forces of the support with various mass of unbalance.

5.3 Effects of Stiffness and Damping Coefficients of Support

Figure 14 that presents the rotor's responses with stiffness coefficient of support K_s=5·10^6 N/m and K_s=5·10^8 N/m displays clearly that stiffness of the support have a vital role when defining the response. Because the responses are directly dependent on the support's stiffness and the contact forces on the responses, the stiffness of the support determinates the behavior of the rotor after the dropdown. This is especially when the friction coefficient is smaller than the threshold friction, like in this case (μ=0.25, C_s=5000 Ns/m). In Figure 14 can be seen that the largest response of the rotor in Y-direction with K_s=5·10^6 N/m comes immediately after the dropdown of the rotor and its value is near to 600 µm. This is absolutely the maximum acceptable value of the responses, because the air gaps of the AMBs were 600 µm. In this case, the responses stabilized quickly unlike in the case of harder supported rotor. This happened despite the fact that the value of relative damping was same in both cases. The orbits of the rotor with various stiffness coefficients of support are presented in Figure 15. Figure 15 shows that displacements of the stiffer case are minimal compared to softer case. This leads to a problem that is presented in Figure 16. The contact forces in the case of K_s=5·10^8 N/m are two times larger than in the case presented in Figure 7 and almost five times larger than in softer supported case. Thus, it is valid to define stiffness coefficient of

support and like this way have an estimation how the system will behave after the emergency dropdown.

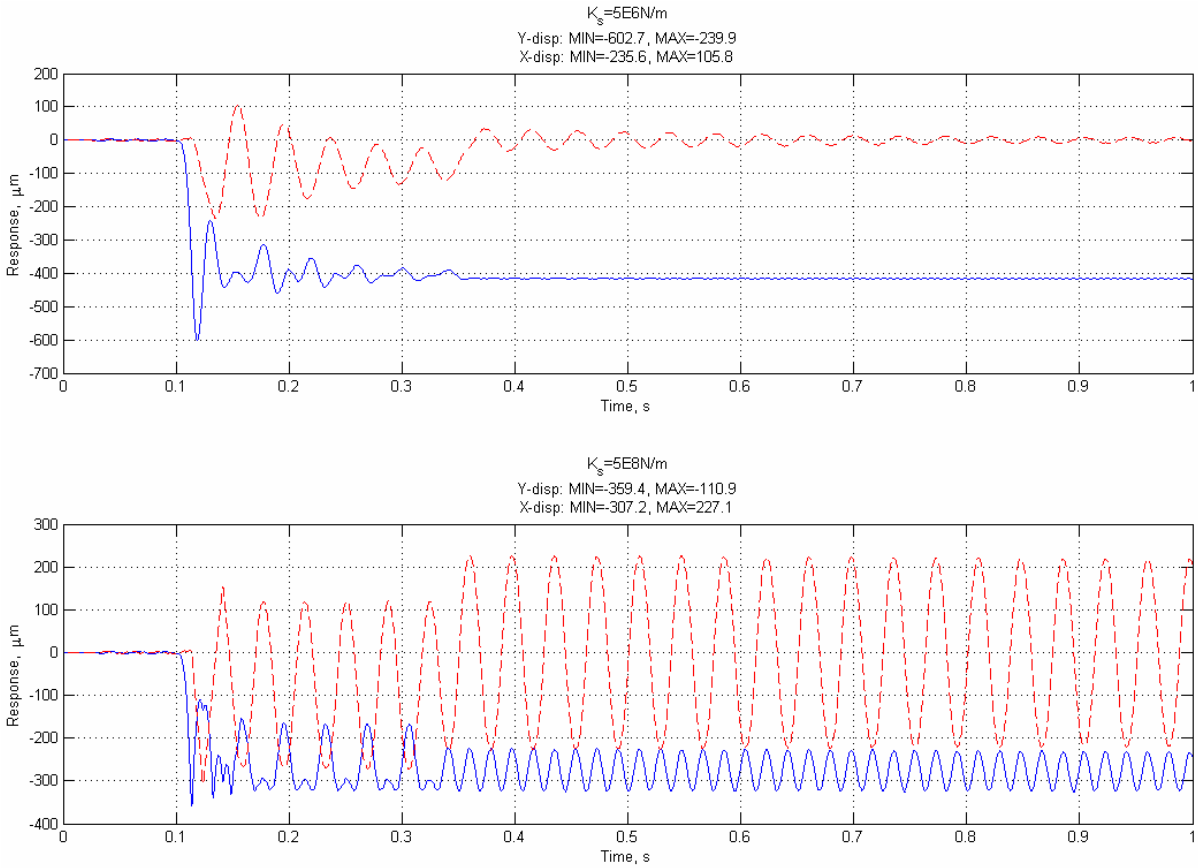

Fig. 14 Responses of the rotor with various stiffness coefficient of support. Solid line indicates *Y*-axis and dash line *X*-axis.

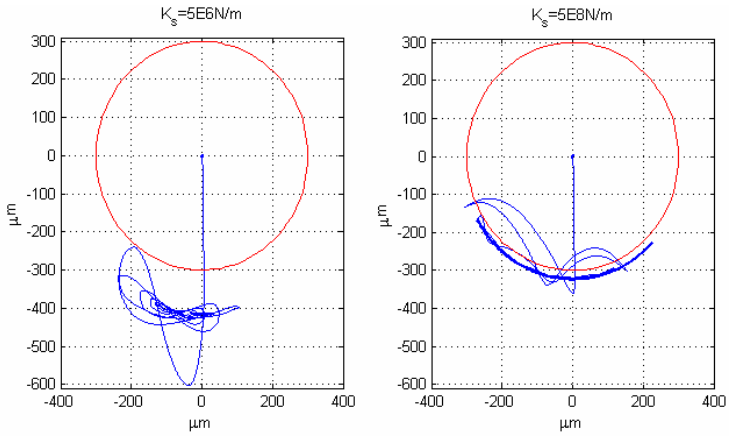

Fig. 15 Orbits of the rotor with various stiffness coefficient of support.

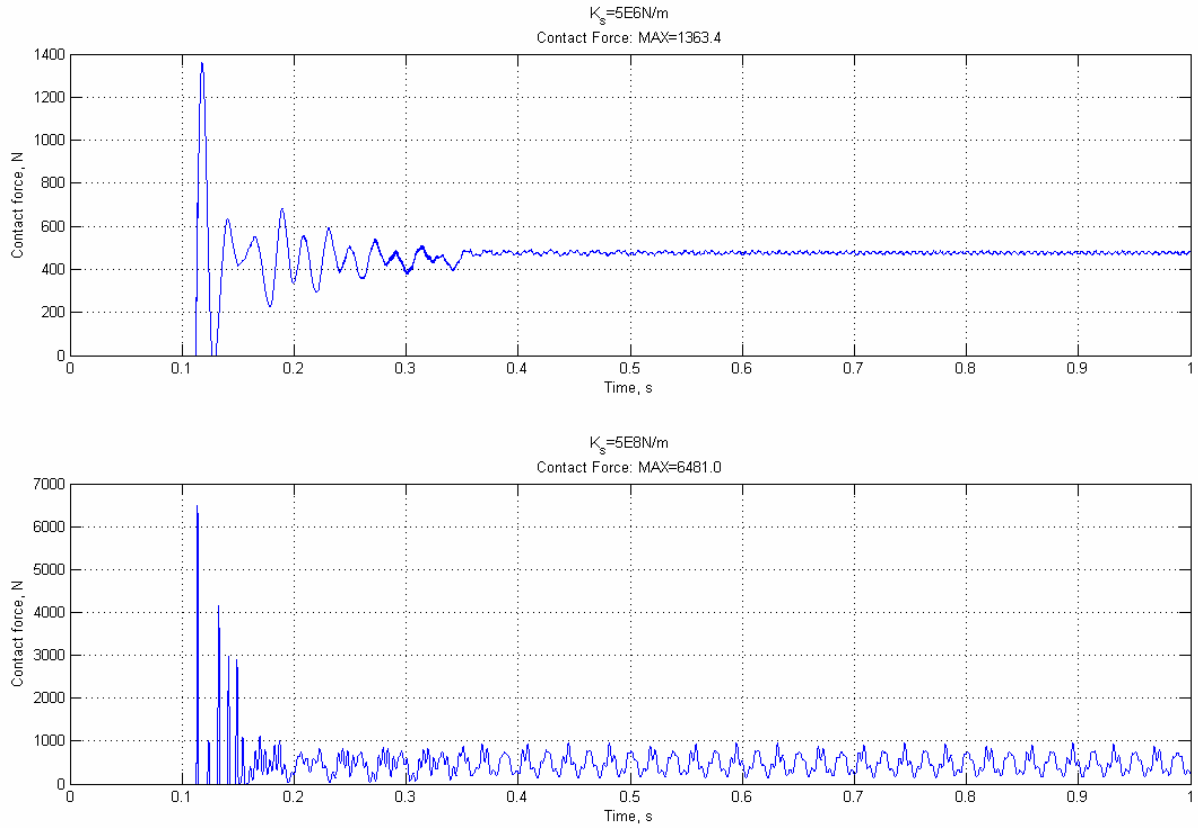

Fig. 16 Contact forces of the support with various stiffness coefficients of support.

As can be seen in Figures 17 and 18, the large support's damping coefficient leads to more stable chaotic response of the rotor after the dropdown, In the more damped case, C_s=27900 Ns/m, the orbit of the rotor is smoother than the low damped case, C_s=2790 Ns/m. This means that vibrations and noises are also smaller in more damped case than in low damped case. Correspondingly, the contact forces stabilize faster in the more damped case than in the low damped case. Based on before mentioned, the importance of damping coefficient with stiffness coefficient is significant.

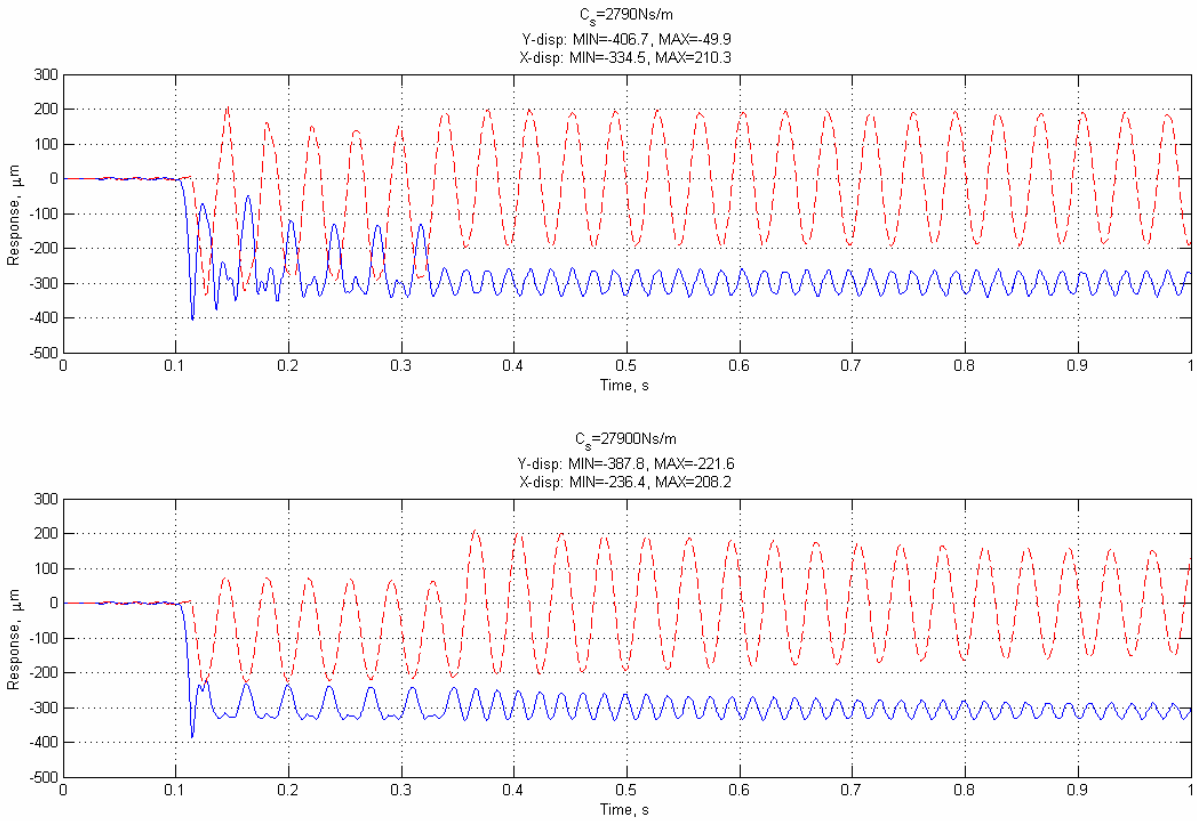

Fig. 17 Responses of the rotor with various damping coefficients of support. Solid line indicates *Y*-axis and dash line *X*-axis.

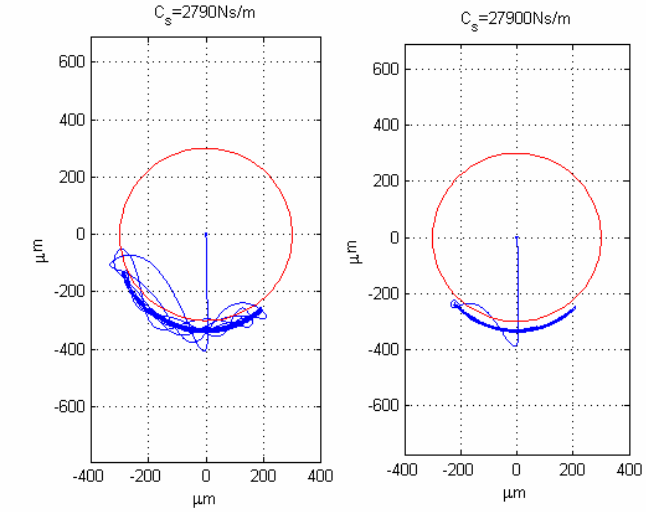

Fig. 18 Orbits of the rotor with various damping coefficients of support.

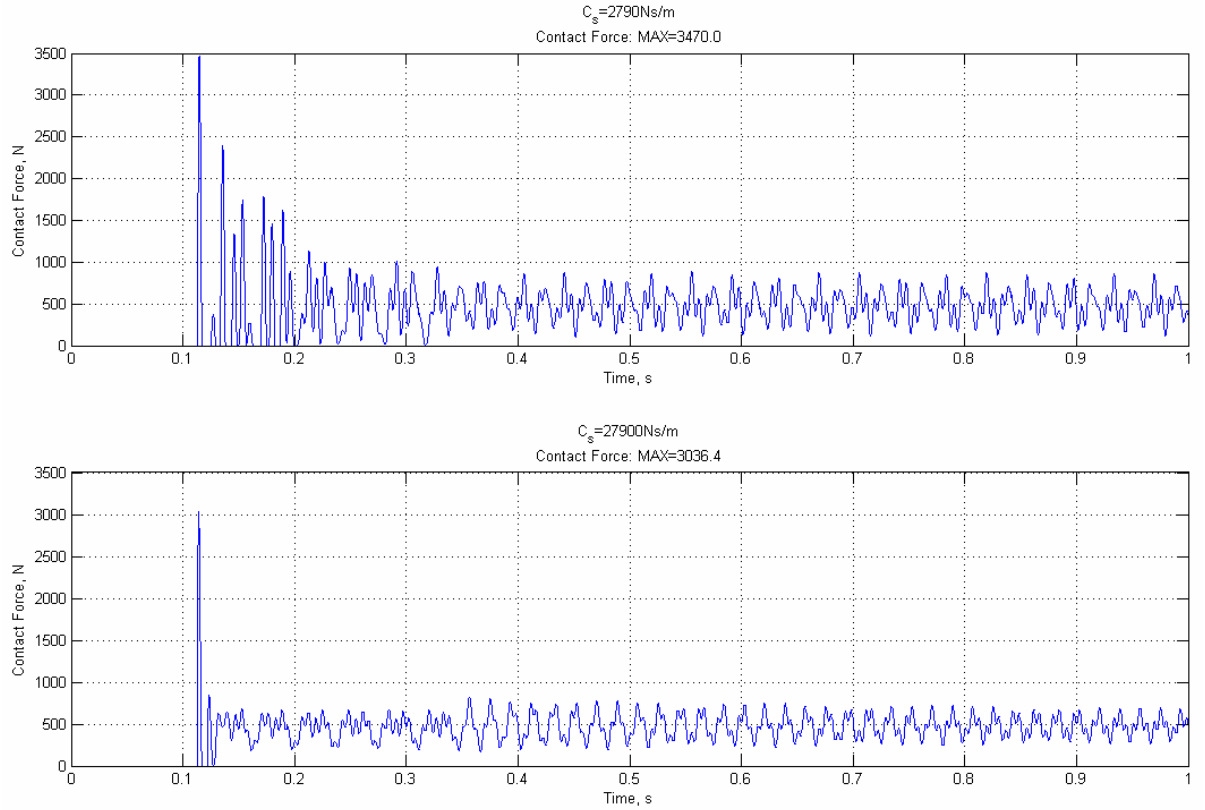

Fig. 19 Contact forces of the support with various damping coefficients of support.

6 CONCLUSIONS

In this study, dynamics of the AMB system during rotor dropdown in the failure incident was investigated using the multibody simulation approach. The studied structure includes the rotor, two AMBs and two retainer ball bearing which included sleeves on the inner rings. Using this model, the effects of retainer bearing parameters on system vibration were examined. The examination of AMB system implies that the multibody simulation approach is a capable procedure for the rotor-retainer bearing simulation. Particularly, the bearing model and the contact models in the multibody approach are efficient and suitable for dropdown simulation.

The results of this paper are in good agreement with studies available in the literature. The AMB system under investigation needs a high friction coefficient between rotor and sleeves in order cause full backward whirling motion of the rotor. This is in agreement with previous examination of AMB [20]. However, it is possible that in practical experiments the rotor can experience whirling motion with lower threshold friction than in the simulations. This is due to the inaccuracies in the friction model. From practically point of view, inaccurate friction

model is due to the use a constant friction coefficient which did not account the increase of the friction coefficient resulting from thermal growing and wearing in sleeves [11]. In the studied system, the rotors unbalance was within the limits of rotor's production precision. Unbalanced mass effected to the behavior of the rotor by slightly deteriorating vibration problem. On the other hand, the stiffness coefficient and the damping coefficient of the support play a vital role in behavior of rotor during and after the rotor's dropdown. Particularly, the contact forces between the rotor and the retainer bearings are dependent on the stiffness of the support. In this study, preload of retainer bearing was ignored since it typically increases the stiffness of bearings. For this reason, in the dropdown situation, the preload can make the orbit of the rotor more chaotic and consequently increase contact forces. Thermal growing compensates the clearance in the bearing during the drop down. It is important to note that preload of bearings makes behavior of the rotor during drop down situation more predictable and may prevent bearing damages.

This research introduces important information for the design of the physical prototype of retainer bearings. The most important results were the critical values for the friction, unbalance, stiffness and damping coefficients. The simulation results also shed a light on the magnitude of the contact forces during the dropdown of the rotor. Multibody simulation proved to be an effective tool when studying the contact dynamics between the rotor and the retainer bearings. The prototype of the studied structure is currently under examination and the results of this research will be verified experimentally in the near future.

REFERENCES

[1] Ishii, T., and Kirk, R. G., 1996, "Transient Response Technique Applied to Active Magnetic Bearing Machinery During Rotor Drop," *ASME Journal of Vibration and Acoustics*, **118**, pp. 154-163.

[2] Schweitzer, G., Bleuler, H., and Traxler, A., 1994, *Active Magnetic Bearings - Basics, Properties and Applications*, vdf Hochschulverlag AG, Zurich.

[3] Orth, M., Erb, R., and Nordmann, R., 2000, "Investigations of the Behavior of a Magnetically Suspended Rotor during Contact with Retainer Bearings," *Proceedings of 7th ISMB*, Zurich, Switzerland, August, ETH Zurich, pp. 33-38.

[4] Fumagalli, M. A., 1997, Modelling and Measurement Analysis of the Contact Interaction between a High Speed Rotor and its Stator, Doctoral Dissertation, Swiss Institute of Technology, Zurich.

[5] Ecker, H., 1998, "Nonlinear Stability Analysis of a Single Mass Rotor Contacting a Rigid Backup Bearing," *Dynamics of Vibro-Impact Systems: Proceedings of the Euromech Colloquium: 15-18 September 1998*, Loughborough, United Kingdom, September, Springer Verlag, pp. 79-89.

[6] Zeng, S., 2002, "Motion of AMB Rotor in Backup Bearings," *ASME Journal of Vibration and Acoustics*, **124**, pp. 460-464.

[7] Cole, M. O. T., Keogh, P. S., and Burrows, C. R., 2002, "The Dynamic Behavior of a Rolling Element Auxiliary Bearing Following Rotor Impact," *ASME Journal of Tribology*, **124**, pp. 406-413.

[8] Raju, K. V. S., Ramesh, K., Swanson, E. E., and Kirk, R. G., 1995, "Simulation of AMB Turbomachinery for Transient Loading Conditions," *Proceedings of MAG'95*, Alexandria, USA, August, Technomics Publishers Co., pp. 227-235.

[9] Swanson, E. E., Kirk, R. G., and Wang, J., 1995, “AMB Rotor Drop Initial Transient on Ball and Solid Bearings,” *Proceedings of MAG'95*, Alexandria, USA, August, Technomics Publishers Co., pp. 207-216.

[10] Wang, X., and Noah, S., 1998, “Nonlinear Dynamics of a Magnetically Supported Rotor on Safety Auxiliary Bearings,” *ASME Journal of Vibration and Acoustics*, **120**, pp. 596-606.

[11] Zeng, S., 2003, “Modelling and Experimental Study of the Transient Response of an Active Magnetic Bearing Rotor during Rotor Drop on Back-Up Bearings,” *Proceedings of the Institution of Mechanical Engineers. Part I, Journal of systems & control engineering*, **217**, pp. 505-517.

[12] Fumagalli, M., and Schweitzer, G., 1996, "Motion of Rotor in Rigid Retainer Bearings," *Proceedings of 5th International Symposium on Magnetic Bearings*, Kanazawa, Japan, August, pp. 509-514.

[13] Sun, G., 2006, “Rotor Drop and Following Thermal Growth Simulation Using Detailed Auxiliary Bearing and Damper Models,” *Journal of Sound and Vibration*, **289**, pp. 334-359.

[14] Kirk, R.G., 1999, ”Evaluation of AMB Turbomachinery Auxiliary Bearings,” *ASME Journal of Vibration and Acoustics*, **121**, pp. 156-161.

[15] ADAMS Online Documentation, 2001, version 12.0, Mechanical Dynamics, Inc, Ann Arbor, Michigan, USA.

[16] Sopanen, J., and Mikkola, A., 2003, ”Dynamic Model of a Deep Groove Ball Bearing Including Localized and Distributed Defects, Part 1: Theory”, *Proceedings of the Institution of Mechanical Engineers, Journal of Multi-Body Dynamics*, **217**(K), pp. 201-211.

[17] Sopanen, J. and Mikkola, A., 2003, ”Dynamic Model of a Deep Groove Ball Bearing Including Localized and Distributed Defects, Part 2: Implementation and Results”, *Proceedings of the Institution of Mechanical Engineers, Journal of Multi-Body Dynamics*, **217**(K), pp. 213-223.

[18] Shabana, A. A., 2001, *Computational Dynamics, 2nd Edition*, John Wiley & Sons, New York.

[19] Shabana, A. A., 1998, *Dynamics of Multibody Systems, 2nd Edition*, John Wiley & Sons, New York.

[20] Foiles, W. C., and Allaire, P. E., 1997, "Nonlinear Transient Modeling of Active Magnetic Bearing Rotors during Rotor Drop on Auxiliary Bearing," *Proceedings of MAG'97*, Alexandria, USA, August, Technomics Publishers Co., pp. 154-163.